Challenging Glass 7
Conference on Architectural and Structural Applications of Glass
Belis, Bos & Louter (Eds.), Ghent University, September 2020.

ISBN 978-94-6366-296-3, https://doi.org/10.7480/cgc.7.4483

On the Low-Velocity Impact Response of Laminated Glass with Different Types of Glass and Interlayers

Alena Zemanová [a], Petr Hála [a], Petr Konrád [a], Jaroslav Schmidt [a], Radoslav Sovják [a], Michal Šejnoha [a]
[a] *Czech Technical University in Prague, Czech Republic, e-mail (alena.zemanova@fsv.cvut.cz)*

An adequate understanding of the response of laminated glass structures to impact loading becomes essential to rationalise their design, which has been proven by several studies that appeared in the last years. Our study focuses on the behaviour of three-layer laminated glass plates subjected to the low-velocity impact of a steel impactor. Using combined experimental and computational analysis, we study the influence of the laminated glass composition on the response of laminated glass, crack initiation, and the final fracture pattern. A polyvinyl butyral or ethylene-vinyl acetate interlayer merges annealed or heat-strengthened soda-lime-silica glass panes together so that the tested panels have the same cross-section layout. As the boundary conditions of the plate largely influence the impact performance of glass panels, the samples were suspended on thin steel ropes to avoid the effect of supports on the laminated glass response. The finite element model of this contact-impact problem, accounting for the time/temperature-dependent behaviour of two polymer interlayers, is presented and validated. Finally, we discuss the effect of the glass and foil type on the contact force and response of laminated glass plates.

Keywords: Laminated glass, Low-velocity impact, Polyvinyl butyral, Ethylene-vinyl acetate, Annealed glass, Heat-strengthened glass, Finite element method

1. Introduction

Laminated glass has exceptional potential to fulfil safety and security demands, as evidenced by its numerous applications for fail-safe, forced-entry, bullet, or blast-resistant elements for engineering, industry, and the military. Besides that, laminated glass is also an attractive material for buildings that are supposed to withstand extreme dynamic loading from natural events, such as seismicity, extreme winds, or other climatic exposures. In its basic configuration, these three-layer composites consist of two glass layers connected with an interlayer, typically made of polymers. Additional layering enables the impact energy to be progressively absorbed and dissipated, even though the ordinary glass is entirely ineffective for such purposes. Thus, the post-breakage resistance of the structural element increases significantly.

Literature review reveals that many of the studies focused on laminated glass under impact loading originates from the field of mechanical engineering and car industry and deals mainly with thin windshields subjected to head impact (Chen et al. 2017). Recently, (Teotia and Soni 2018) provided a review focused on the finite element analysis of laminated glass under impact and blast loading. For the polymer interlayer description, different constitutive laws were tested, such as a viscoelastic generalised Maxwell model (Hána et al. 2019), an elastic model with shear modulus adjusted for given loading time, or even a hyperelastic models taking into account possible finite strains in the polymer foil (Pelfrene et al. 2018). If also the response after glass fracture is analysed, the simplest way is to combine the element deletion or erosion method with a local Rankine criterion (Pelfrene et al. 2016b). As shown in (Song et al. 2008) and in (Pelfrene et al. 2016a) for glass plates, this approach can lead to instabilities in the simulation as the energy is dissipated within an element suddenly which causes stress oscillations in the neighbouring elements. To overcome this drawback, the authors try to use non-local models initially developed for concrete or to adjust the Rankine base criterion to a nonlocal one (Pyttel et al. 2011) or (Alter et al. 2017). Besides the classical finite element method, also different approaches, e.g., the extended finite element method or discrete element method, can be found in the literature (Wang et al. 2017). The detail numerical model, describing each layer of the laminated glass, can be reduced and approximated using an equivalent monolithic model or a smeared model consisting from two superimposed shells with adjusted thicknesses, e.g., (Timmel et al. 2007) or (Peng et al. 2013). Simple models representing the impactor and the glass sample by the system of masses and springs can be derived (Janda et al. 2020) to estimate contact forces and global response of the sample. Practical models for post-glass breakage response of laminated heat-treated glass are proposed and discussed in (Galuppi and Royer-Carfagni 2018), but so far for static loading.

In this study, the basic configuration of laminated glass, consisting of two glass plies and a polymer interlayer, is tested under impact loading. In the first section, the experimental study is presented, and the behaviour of monolithic and laminated glass samples is compared. Further, the response in terms of velocities and contact forces is analysed

numerically. We rely on the conventional finite element method as it is the dominant framework in solvers for practical engineering problems. Finally, the conclusions from the combined analysis are summarised.

2. Experimental study

The experimental study was performed on different types of samples: a single monolithic panel made of annealed glass (ANG), and three laminated glass samples consisting of annealed glass plies and a polyvinyl butyral foil (ANG-PVB), annealed glass plies and an ethylene-vinyl acetate interlayer (ANG-EVA), and heat-strengthened glass plies and a polyvinyl butyral foil (HSG-PVB). The in-plane dimensions of the plates were 1.5 m × 1.5 m with the nominal thickness of 10 mm for the monolithic plate, 5 mm for each glass layer in laminated glass and 0.76 mm for the interlayer. The EVA-based foil was EVALAM 80-120 and PVB-based TROSIFOL BG R20.

As we wanted to minimise the effect of boundary conditions on the response of laminated glass, the samples were suspended on thin steel strings, see Fig. 1. This way, the results are not affected by a possible compression or damping in the rubber bands conventionally placed between the glass and frame to avoid stress concentrations.

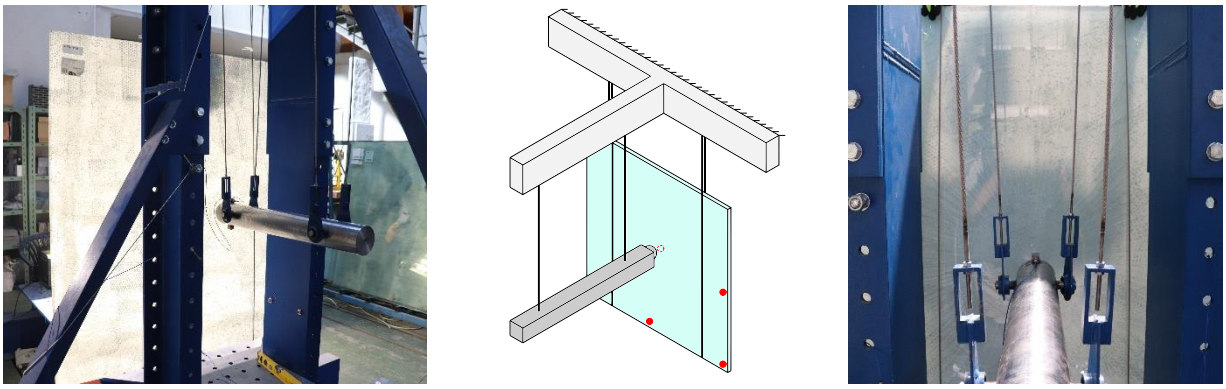

Fig. 1 Photos of the experimental set-up and scheme of the sample and impactor with positions of accelerometers.

The impactor was made of a steel cylinder with a weight of 48.7 kg and with a hard hemispherical nose hitting the squared glass sample at the centre. The response of glass samples and impactor was recorded by five piezoelectric accelerometers adhesively mounted on a quarter of the plate and screwed on the head of the impactor, Fig. 1. The measurements were done for impact energies corresponding to different heights of the impactor, i.e., 3, 30, 50, 70, and finally 100 cm relatively to the plate centre. The first tests were non-destructive to compare the response and contact forces of monolithic and laminated glass samples. Then, the height of the impactor release was increased until the glass fracture. The results of both the non-destructive and destructive tests are analysed in the next two sections.

2.1. Non-destructive testing

The experimental testing for the low impact height of 3 cm enabled the comparison of the response of all four samples. As all three laminated samples for the impact height of 30 cm were without any visible crack or defect, the results are presented in this section as well.

After the impact, the unsupported plate starts to move and vibrate. Its dynamic response is superimposed from several vibration modes. As the square plate was impacted at the centre, we assume that the excited modes are bi-axially symmetric. This assumption was verified by comparing experimentally obtained accelerations recorded in the middle of the vertical and horizontal edges of the glass plates subjected to the impact loading. These double-symmetric mode shapes with appropriate frequencies, corresponding to the third, eighth, fourteenth, and nineteenth vibration mode, are shown for monolithic glass 10 mm thick in Fig. 3. The first six modes corresponding to the rigid body motions were skipped. The natural frequencies identified for monolithic glass from both, experimental analysis, using a roving hammer test, and numerical modal analysis for an unsupported square plate were compared. The differences in values were less than 1%, and therefore, only the experimental frequencies are reported. The comparison also proved that the thin strings supported the plate did not affect the response significantly.

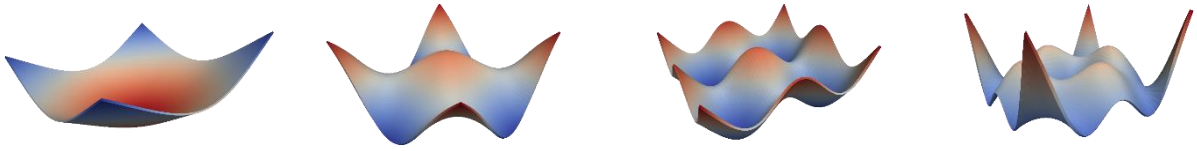

3. mode, frequency 26.3 Hz | 8. mode, frequency 72.3 Hz | 14. mode, frequency 135 Hz | 19. mode, frequency 188 Hz

Fig. 3 Double-symmetric mode shapes and corresponding natural frequencies of the squared monolithic glass plate 10 mm thick (ANG).

Using the Fast Fourier Transform (FFT), we analysed the signals from accelerometers placed on the glass samples after the impact. The FFT analysis for the accelerations of the corner is shown in Fig. 4. For monolithic glass ANG, three significant frequencies (for the 8th, 14th, and 19th modes) complemented with several lower peaks are visible from the signal analysis, whereas for laminated glass, the dominant frequency corresponds to the 3rd mode and the others are damped by the interlayer. For all three laminated samples, the dominant frequency is higher than those for monolithic glass plate with a thickness of 10 mm. For ANG-PVB, the frequency is equivalent to that for a glass plate 10.76 mm thick. The impact from the height of 3 cm was repeated three times, and the values of frequencies are consistent. For the impact height of 30 cm, the shapes of the plots are the same, and just the magnitudes are higher for higher impact energies.

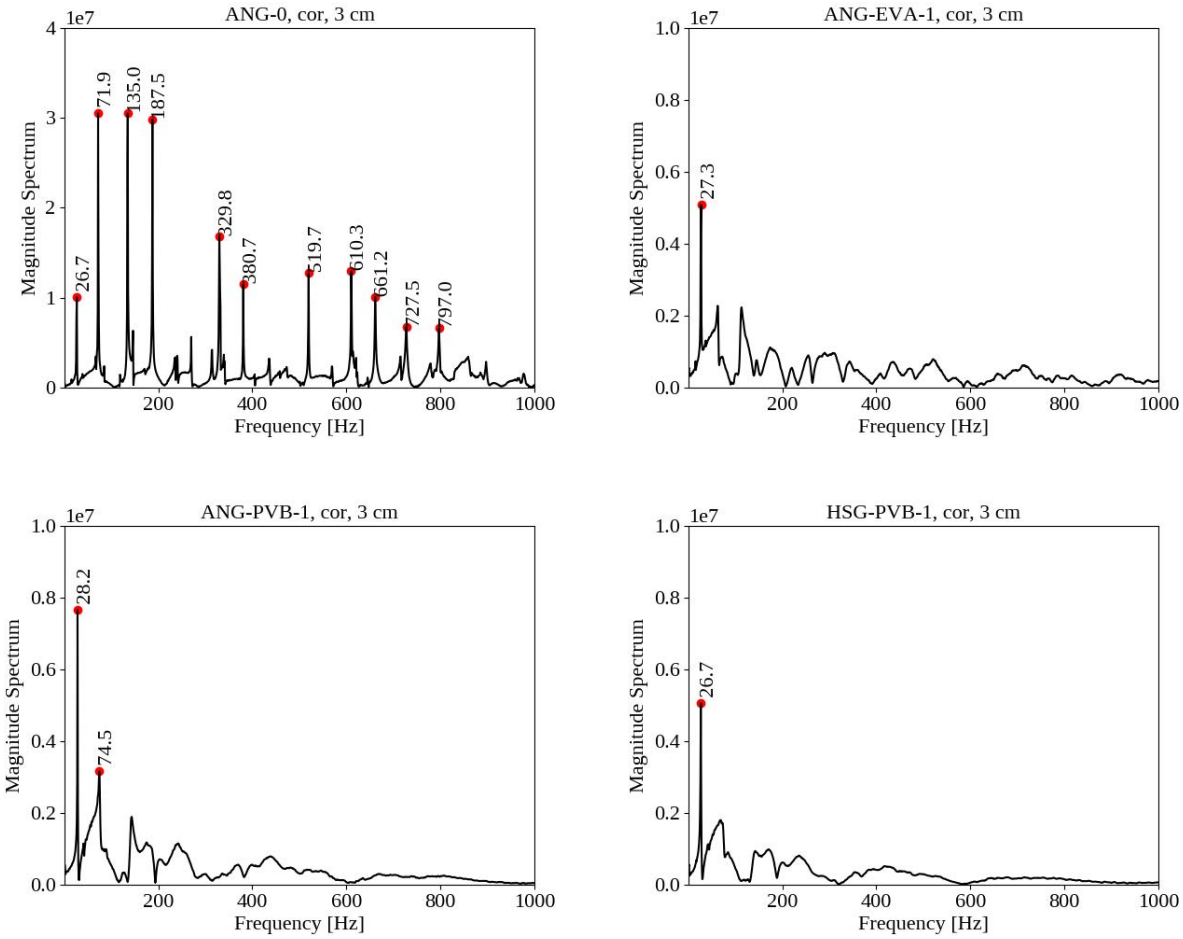

Fig. 4 FFT analysis of the signal from the accelerometer in the corner of a monolithic or laminated glass sample.

Table 1 summarises the frequencies obtained by the experimental modal analysis (EMA) using a roving hammer test and the dominant ones from the signal analysis after the impact of the steel impactor (48.7 kg). The differences in dominant frequencies of laminated samples are about 5%. Except for the effects of the interlayer material, the slightly different actual thicknesses of the samples due to manufacturing tolerance limits could partially cause these differences. In the case of HSG, the frequency could also be influenced by the initial residual stresses.

Table 1: Comparison of natural frequencies.

Specimen	Thicknesses [mm]	Frequency from EMA [Hz]				Dominant frequencies [Hz]			
		3.	8.	14.	19.	From signals after impact			
ANG	10	26.3	72.3	135	188	26.7	71.9	135	188
ANG-EVA	5/0.76/5	27.1	76.2	–	147	27.3			
ANG-PVB	5/0.76/5	28.5	75.6	142	194	28.2			
HGS-PVB	5/0.76/5	Not tested				26.7			

The response of samples in terms of velocities integrated from accelerations of selected points is shown in Fig. 5 for the impact duration. The comparison of monolithic and laminated glass proves that both foils damped the response as

the vibrations corresponding to higher frequencies were suppressed. As expected, the heat strengthening of glass did not change the response significantly. The velocities of samples with PVB foil are similar to that of monolithic glass, just the fluctuations and peaks corresponding to higher vibration modes are invisible. The response of the sample with EVA foil is not only smoothed but also shifted in time. The velocities at the midpoint of the side edge (sid) and the midpoint of the bottom edge (bot) are almost indistinguishable. Therefore, the suspension did not affect the response significantly, and only a quarter of an unsupported plate will be analysed numerically. For the impact height of 3 cm, the laminated glass samples were tested three times. The experimental testing provides consistent responses as a meaningful match of the velocities from three tests for the same laminated glass sample can be seen in the graphs on the left side of Fig. 5.

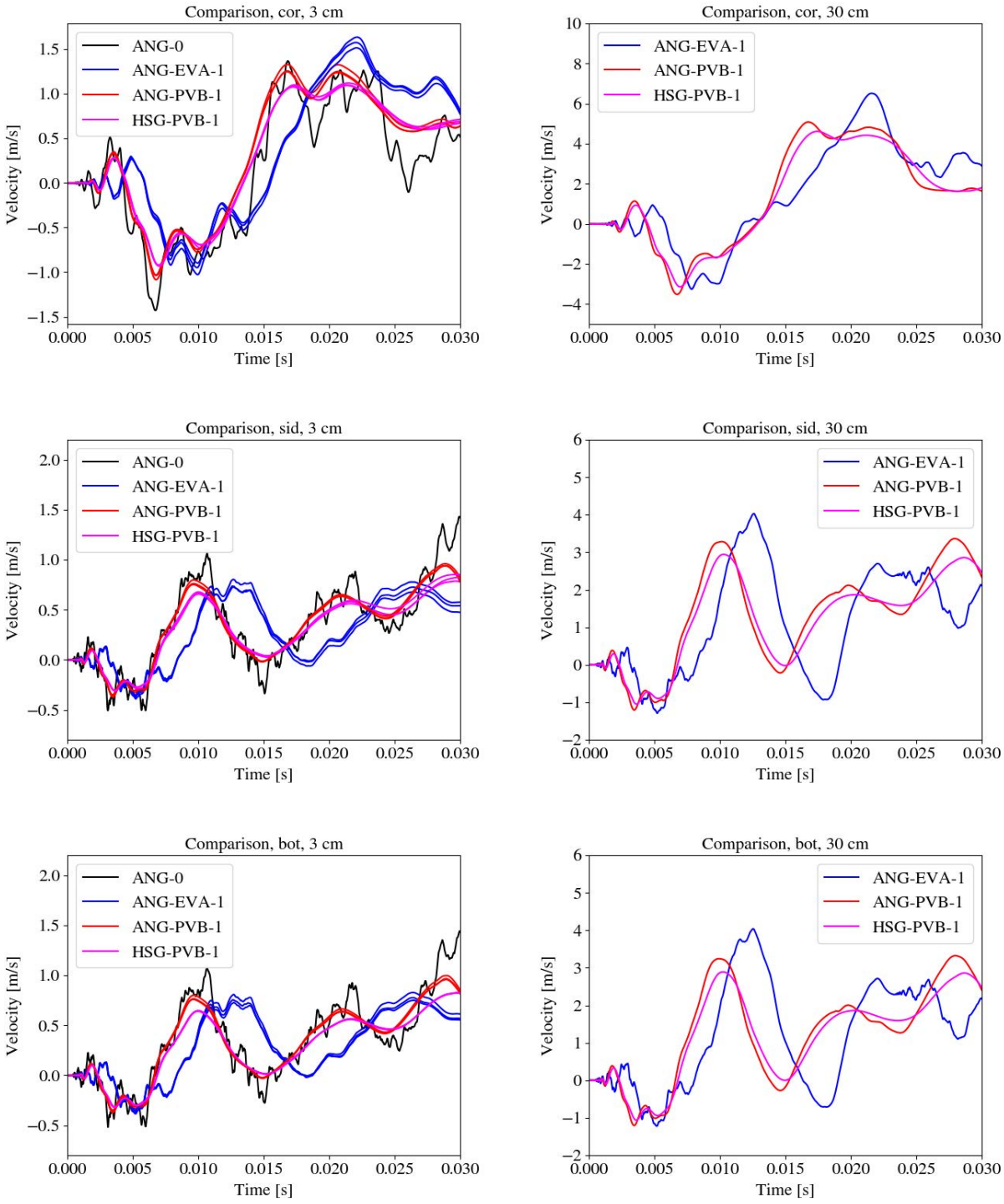

Fig. 5 Velocities at the corner (cor), at the midpoint of the side edge (sid), and at the midpoint of the bottom edge (bot) for monolithic (ANG-0) and laminated (ANG-EVA, ANG-PVB, and HSG-PVB) glass samples for the impact height 3 cm or 30 cm.

The velocities at the centre of the plate are shown for the lowest impact height only in Fig. 6 as the central accelerometer frequently peeled off, or the signal was out of the measurement range for higher impact heights.

The contact forces were derived from the response of the impactor during the contact multiplying the accelerations of the head by the mass of the impactor. The filter CFC 1000 was applied to the data to reduce the noise, e.g., (Alter et al. 2017). The evolution of the contact force during the contact is shown in Fig. 7. The highest peak of the contact force corresponds to the monolithic glass as its response is superimposed only from a few vibration modes. These oscillations are visible also after the contact for laminated samples, but they are damped, and the contact force evolution is smoother than that for monolithic glass. The longest contact corresponds to the impact on the sample with EVA foil. The PVB-based laminated glass plates behave similarly to the monolithic glass. For all laminated glass plates, the peak values of the contact force are lowered due to the polymer foil compared to the monolithic glass sample.

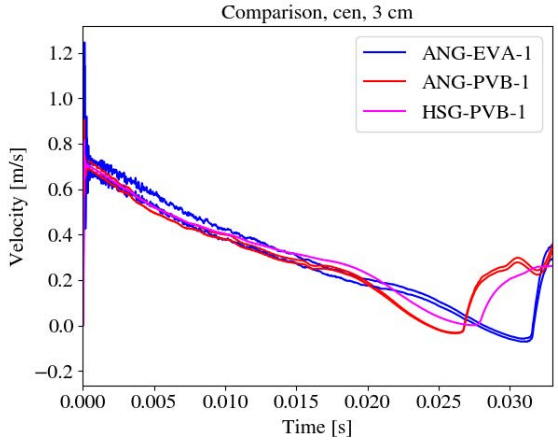

Fig. 6 Velocities at the centre of the plate (cen) for monolithic (ANG-0) and laminated (ANG-EVA, ANG-PVB, and HSG-PVB) glass samples for the impact height 3 cm.

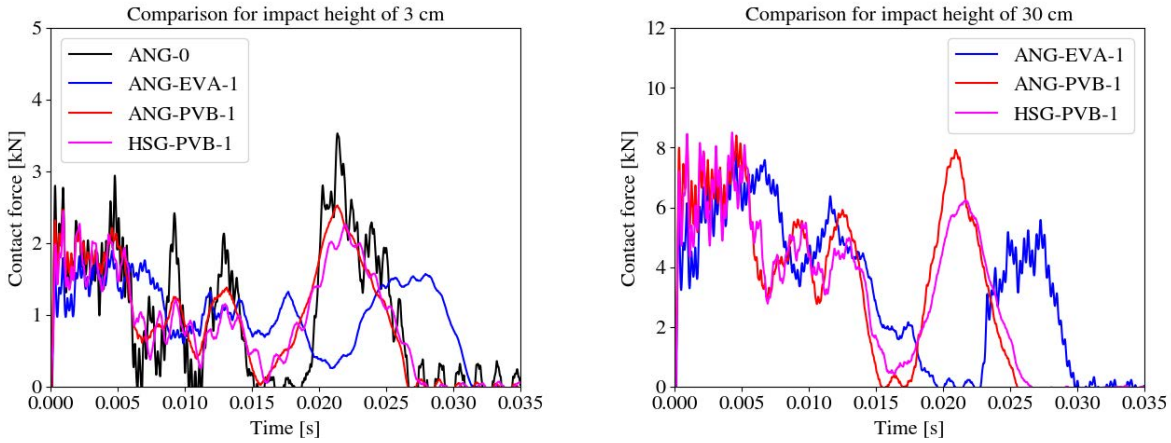

Fig. 7 Contact forces from experimental measurement derived from accelerations of the impactor for monolithic (ANG-0) and laminated (ANG-EVA, ANG-PVB, and HSG-PVB) glass samples for the impact height 3 cm or 30 cm.

2.2. Destructive testing

Table 2 shows how the laminated glass samples responded to the impact of different energies.

Table 2: Summary of destructive tests on laminated glass samples.

Specimen	Thicknesses	Temperature	Impact height / Impact energy			
	[mm]	[°C]	0.3 m / 143 J	0.5 m / 239 J	0.7 m / 334 J	1.0 m / 478 J
ANG-EVA-1	5/0.76/5	26.1	No visible crack	Fractured	–	–
ANG-PVB-1	5/0.76/5	26.5	No visible crack	No visible crack	No visible crack	Fractured
HGS-PVB-1	5/0.76/5	27.6	No visible crack	No visible crack	No visible crack	Fractured

We increased the impact height gradually from 3 cm to 30, 50, 70, or 100 cm. The samples with PVB foil resisted to the impact from the height of 70 cm without any visible crack. Then for the impact corresponding to the height of the impactor 100 cm, both glass plates fractured and most of the glass shards stayed attached on the interlayer without any visible signs of delamination. The glass was crushed and fell away only in a small area where the impactor hit the plate. The annealed and heat-strengthened glass fractured under the same impact energy, so no visible improvement of the resistance was observed for this test. The sample with EVA-foil failed at the lowest impact height of 30 cm. For comparison, the monolithic single-layer glass plate was broken for the height of the impactor of 14 cm.

The contact force for two non-fractured and one fractured laminated glass panels is shown in Fig. 8. As can be seen from the recorded data, the peaks of the contact force were lower for the EVA-based sample than for the PVB-based ones, even though the sample with EVA was damaged for the lowest impact energy. Therefore, the reason could be a slightly smaller real thickness of the glass layers or a higher level of the initial micro defects and cracks.

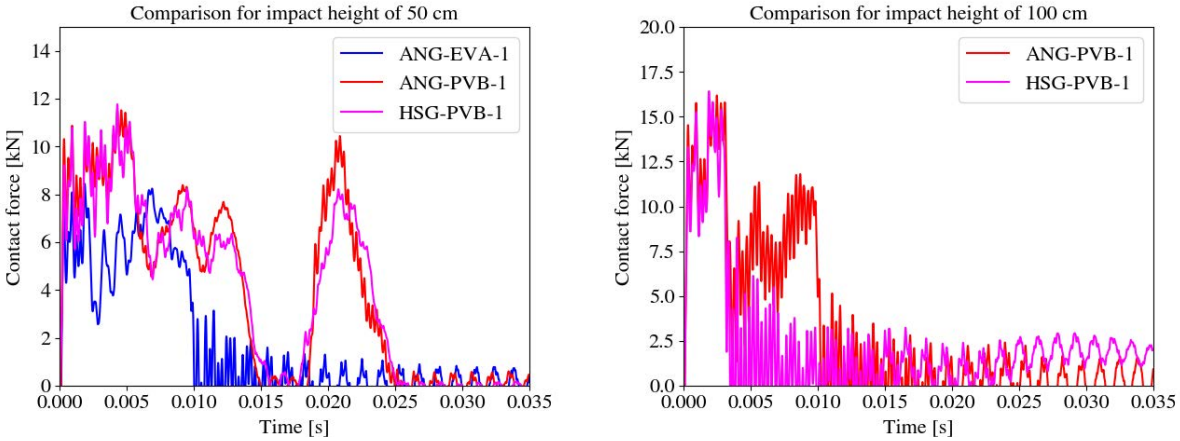

Fig. 8 Contact forces derived from the accelerations of the impactor for non-fractured and fractured laminated glass samples. ANG-EVA-1 fractured for impact height 50 cm (left), ANG-PVB-1 and HSG-PVB-2 fractured both for 50 cm (right).

The final fracture patterns for laminated glass samples are shown in Fig. 9. For both samples with annealed glass plies, the pattern is similar. The radial cracks were initially evenly distributed around the contact zone. The more the head of the impactor penetrated the plate, the more cracks appeared near the diagonals creating an X-shaped band visible in Fig. 9 a) and b). Due to the residual stresses, the heat-strengthening sample was damaged by a denser network of cracks that branch, Fig. 9 c).

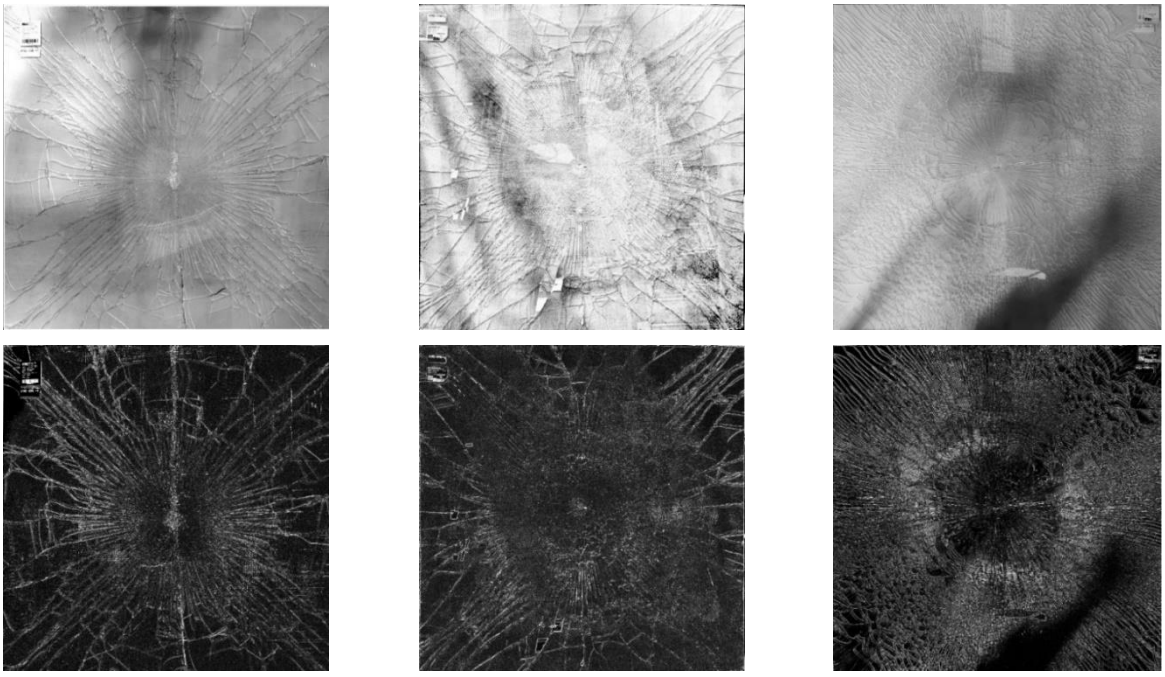

a) ANG-EVA-1 b) ANG-PVB-1 c) HSG-PVB-1

Fig. 9 Photos of laminated glass samples after fracture and fracture pattern using an edge detection algorithm

3. Numerical modelling

As the experimental tests have been done so far on a limited number of samples, we built a finite element model to predict the response of laminated glass plates that could be further used for a parametric study. In this section, the first part is focused on the response of laminated glass panels before the glass fracture. Then, the future extension of the model to capture the crack initiation and propagation is briefly introduced.

3.1. Laminated glass without glass fracture

The numerical analysis of the impactor and laminated glass plate was carried out using a commercial finite element package LS-DYNA (Hallquist 2006). For impact simulations, the explicit time-integration scheme in LS-DYNA is based on a modified central difference method. The interlayer and glass plies were discretised with fully integrated brick elements, whereas for the impactor, the fully integrated quadratic shell elements were employed. The element size was about 2.5 mm. Assuming that the effect of the thin steel ropes on the response of glass plate during the impact is negligible, only a quarter of the plate and impactor with symmetry conditions was utilised. A penalty-based contact without friction was defined between the head of the steel impactor and the glass ply to eliminate the penetration. In this approach, forces proportional to the penetration depth are applied to minimise interpenetration between the bodies in contact.

Table 3: Material parameters for the impactor, glass, and polymers.

Material	Density [kg/m^3]	Young's modulus [GPa]	Poisson ratio [–]	Bulk modulus [GPa]
Steel	1,614,087	210	0.3	–
Glass	2,500	72	0.22	–
EVA	950	GMM (Hána et al. 2019)	–	2.0
PVB	1,100	GMM (Hána et al. 2019)	–	2.0

Regarding the material parameters, glass was assumed to behave like an isotropic elastic material and steel as a rigid shell with Young's moduli, Poisson ratios, and densities, according to Table 3. As only the hemispherical head represented the impactor to reduce the number of elements, the density of steel was adjusted to obtain the whole mass of the impactor. A viscoelastic generalised Maxwell model (GMM) approximated the time/temperature-dependent response of polymer foil, combined with the Williams-Landel-Ferry shift parameters according to (Hána et al. 2019). The corresponding shear moduli for both foils and three different temperatures are shown in Fig. 10. It can be seen that the PVB foil is more temperature-sensitive, provides higher shear coupling for loading with a short duration, but the shear modulus decreases significantly during long-term loading. The densities and bulk moduli of both polymers are again shown in Table 3. We also tried to model the interlayer as an elastic material with the shear moduli corresponding to the initial shear modulus of the generalised Maxwell model which provided worse results than the viscoelastic model for EVA-based samples and quite similar response for PVB-based samples. As the interlayer is often assumed to be a hyperelastic material in the literature, we also tested a simple model for nearly incompressible continuum rubber (Blatz-Ko). The response of the rubber was the same as that of the elastic model.

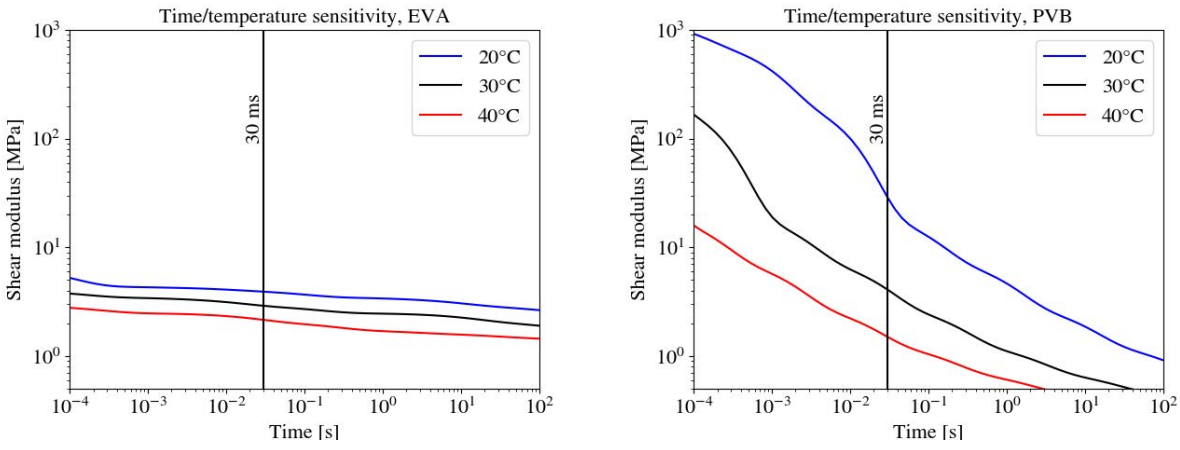

Fig. 10 Shear modulus of EVA and PVB interlayer in the time domain for two different temperatures.

The response of samples ANG-EVA-1 and ANG-PVB-1 in terms of velocities integrated from accelerations of two points, at the corner and the midpoint of the side edge, is shown in Fig. 11 for the impact height of 30 cm. The acceleration of the centre of laminated glass plates was not measured, and the acceleration of the midpoint of the bottom edge coincides with that of the midpoint of the side edge. For all velocities, we achieved a good agreement

between the experimental data and the numerical prediction. The time-evolution of predicted velocities corresponds to the measured data, but the positions of local extremes are slightly shifted for ANG-PVB-1. The differences in the response of the PVB-based sample against the EVA-based laminated glass were captured very well by the numerical model.

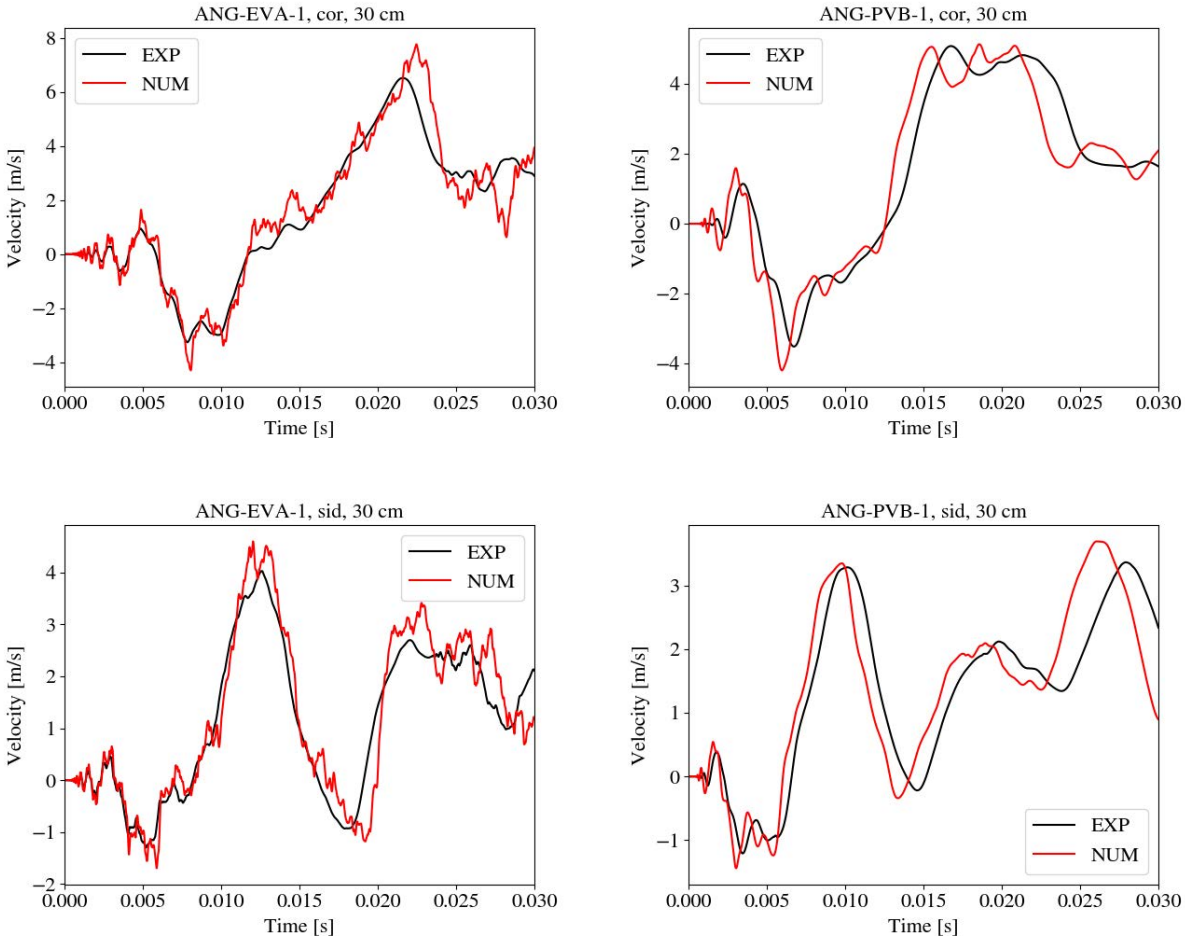

Fig. 11 Validation of velocities from numerical analysis (NUM) against experimental data (EXP) at the corner of the plate (cor) and the centre of side edge (sid) for ANG-EVA and ANG-PVB samples for the impact height of 30 cm.

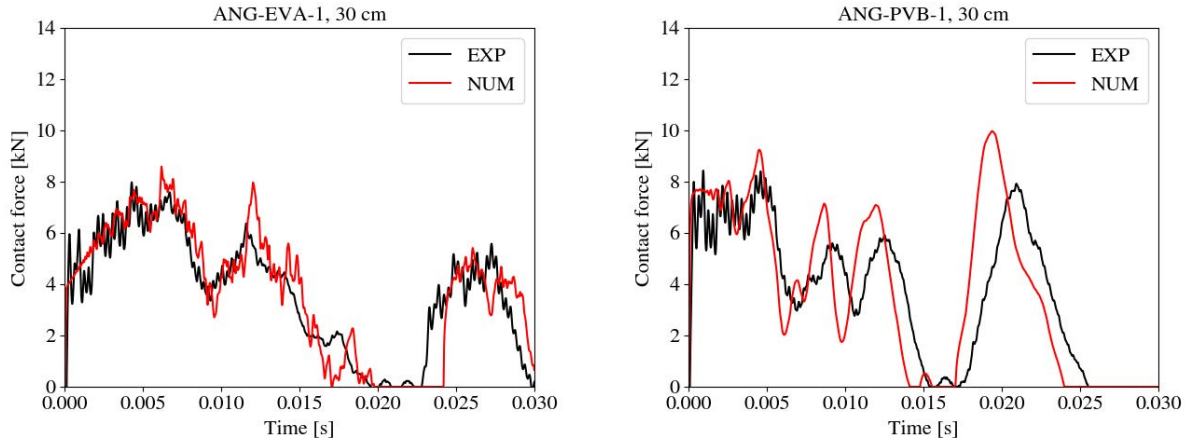

Fig. 12 Validation of contact forces from numerical analysis (NUM) against experimental data for contact force (EXP) derived from the accelerations of the impactor for laminated glass samples for the impact height of 30 cm.

The contact forces were derived from the accelerations of the impactor during the contact. The filter CFC 1000 was again applied to the data to reduce the noise, e.g., (Alter et al. 2017). The validation against experimental data in Fig. 12 again shows a reliable numerical prediction of the contact force for EVA-based sample with a slightly shifted last contact. The peaks of contact forces were overestimated for the PVB-based sample. The reason for this could be a

stiffer response of PVB interlayer due to a slightly overestimated shear modulus. Note that the Prony series for the generalized Maxwell model corresponds to an optimal fit of measured moduli, but the measured values of shear modulus can differ from specimen to specimen, see (Hána et al. 2019). Nevertheless, the model predicted the impact duration, the contact force evolution, and the positions of local peaks well.

3.2. Description of glass fracture

The next step is the extension of the numerical model to provide the fracture response of glass. To this purpose, we will use two damage models.

First, we are going to test a smeared fixed crack model implemented in LS-DYNA with a brittle, stress-state dependent failure criterion. If the maximum principal stress reaches the value of the tensile strength of glass according to the Rankine stress criterion, a crack occurs perpendicular to the maximum principal stress direction. Then, the appropriate stress and stiffness tensor components are reduced in a few time steps or by a damage model. This fixed crack model can incorporate up to two orthogonal cracks per integration point, the crack closure effects are treated, and a local or a nonlocal failure criterion can be defined.

Second, a phase-field damage model will be employed. This approximation of brittle fracture can be seen as a generalisation of Griffith's theory, where the sharp crack is regularised. The displacement field and the crack evolution is predicted by the minimisation of the total potential energy, and no other assumption for cracks initiation is needed. Different formulation and extensions can be found in the literature. We plan to test the classical formulation with the energy-based driving force, for plates see (Kiendl et al. 2016), or its modified versions with a Rankine-based stress criterion, (Miehe et al. 2015).

As a fine mesh and longer computational time are needed, especially for the phase-field models for such large laminated glass samples, the numerical results and the comparison will be presented separately.

4. Conclusions

Let us summarise the following conclusions based on this experimental study on a limited number of samples combined with a numerical analysis of laminated glass plates under impact loading:

- The experimental study proved that the polymer foil damped the vibrations corresponding to higher natural frequencies and modal shapes. Therefore, the response of the laminated glass sample and the time evolution of the contact force were smoothed, and the peak value of the contact force was reduced in comparison to that for the monolithic glass plate.
- The laminated glass sample with EVA foil fractured under lower impact energy than the samples with the PVB interlayer. However, this could be caused by a slightly smaller real thickness of the glass layer or by a higher level of the initial micro defects and cracks on the surface, as the extreme values of the measured contact force were not higher.
- Regarding heat-strengthening, no visible improvement of the resistance was observed for our experimental set-up, as the annealed and heat-strengthened glass fractured under the same impact energy. The final fracture pattern differed significantly. In future experimental tests, we are going to refine the number of tested impact heights to increase the energy in smaller jumps and further study the effect of heat-strengthening on the impact resistance.
- We validated the proposed finite element model against the experimental data. For both samples with EVA or PVB foils, the numerical prediction of the response of the laminated glass plate and the evolution of the contact force matched the experimental response well; the impact duration and the positions of local peaks of contact force were predicted correctly, but the largest values of the contact force were overestimated for the PVB-based sample.

At this moment, the conclusions are limited by the fact that one sample for each material combination was tested. We will extend this study and analyse twelve laminated glass samples in total (3 for each configuration). Even though this number is still limited for statistical analyses of the state of glass fracture, as the tensile strength in bending can vary significantly, the results will provide a better insight into the non-destructive analysis and validation of the numerical model, which will be used for further parametric studies.

5. Acknowledgements

The financial support from the Czech Science Foundation provided through the grant No. 19-15326S is gratefully appreciated. We would also like to thank Tomáš Plachý from Czech Technical University in Prague for performing the experimental modal analysis, briefly reported in this study.

6. References

Alter, C., Kolling, S., Schneider, J.: An enhanced non–local failure criterion for laminated glass under low velocity impact. Int. J. Impact Eng. 109, 342–353 (2017). https://doi.org/10.1016/J.IJIMPENG.2017.07.014

Chen, S., Zang, M., Wang, D., Yoshimura, S., Yamada, T.: Numerical analysis of impact failure of automotive laminated glass: A review. Compos. Part B Eng. 122, 47–60 (2017). https://doi.org/10.1016/J.COMPOSITESB.2017.04.007

Galuppi, L., Royer-Carfagni, G.: The post-breakage response of laminated heat-treated glass under in plane and out of plane loading. Compos. Part B Eng. 147, 227–239 (2018). https://doi.org/10.1016/j.compositesb.2018.04.005

Hallquist, J.: LS-DYNA® theory manual. (2006)

Hána, T., Janda, T., Schmidt, J., Zemanová, A., Šejnoha, M., Eliášová, M., Vokáč, M.: Experimental and Numerical Study of Viscoelastic Properties of Polymeric Interlayers Used for Laminated Glass: Determination of Material Parameters. Materials (Basel). 12, 2241 (2019). https://doi.org/10.3390/ma12142241

Janda, T., Zemanová, A., Hála, P., Konrád, P., Schmidt, J.: Reduced order model of glass plate loaded by low-velocity impact. Int. J. Comput. Methods Exp. Meas. 8, 36–46 (2020). https://doi.org/10.2495/CMEM-V8-N1-36-46

Kiendl, J., Ambati, M., De Lorenzis, L., Gomez, H., Reali, A.: Phase-field description of brittle fracture in plates and shells. Comput. Methods Appl. Mech. Eng. 312, 374–394 (2016). https://doi.org/10.1016/j.cma.2016.09.011

Miehe, C., Schänzel, L.-M., Ulmer, H.: Phase field modeling of fracture in multi-physics problems. Part I. Balance of crack surface and failure criteria for brittle crack propagation in thermo-elastic solids. Comput. Methods Appl. Mech. Eng. 294, 449–485 (2015). https://doi.org/10.1016/J.CMA.2014.11.016

Pelfrene, J., van Dam, S., Sevenois, R., Gilabert, F., van Paepegem, W.: Fracture simulation of structural glass by element deletion in explicit FEM. In: Challenging Glass Conference Proceedings - Challenging Glass 5: Conference on Architectural and Structural Applications of Glass, pp. 439–454 (2016)(a)

Pelfrene, J., van Dam, S., Spronk, S., van Paepegem, W.: Experimental Characterization and Finite Element Modelling of Strain-rate Dependent Hyperelastic Properties of PVB Interlayers. In: Challenging Glass 6: Conference on Architectural and Structural Applications of Glass, pp. 435–446. TU Delft Open (2018)

Pelfrene, J., Kuntsche, J., Van Dam, S., Van Paepegem, W., Schneider, J.: Critical assessment of the post-breakage performance of blast loaded laminated glazing: Experiments and simulations. Int. J. Impact Eng. 88, 61–71 (2016)(b). https://doi.org/10.1016/j.ijimpeng.2015.09.008

Peng, Y., Yang, J., Deck, C., Willinger, R.: Finite element modeling of crash test behavior for windshield laminated glass. Int. J. Impact Eng. 57, 27–35 (2013). https://doi.org/10.1016/j.ijimpeng.2013.01.010

Pyttel, T., Liebertz, H., Cai, J.: Failure criterion for laminated glass under impact loading and its application in finite element simulation. Int. J. Impact Eng. 38, 252–263 (2011). https://doi.org/10.1016/j.ijimpeng.2010.10.035

Song, J.-H., Wang, H., Belytschko, T.: A comparative study on finite element methods for dynamic fracture. Comput. Mech. 42, 239–250 (2008). https://doi.org/10.1007/s00466-007-0210-x

Teotia, M., Soni, R.K.: Applications of finite element modelling in failure analysis of laminated glass composites: A review. Eng. Fail. Anal. 94, 412–437 (2018). https://doi.org/10.1016/J.ENGFAILANAL.2018.08.016

Timmel, M., Kolling, S., Osterrieder, P., Du Bois, P.A.: A finite element model for impact simulation with laminated glass. Int. J. Impact Eng. 34, 1465–1478 (2007). https://doi.org/10.1016/j.ijimpeng.2006.07.008

Wang, X. er, Yang, J., Liu, Q. feng, Zhang, Y. mei, Zhao, C.: A comparative study of numerical modelling techniques for the fracture of brittle materials with specific reference to glass. Eng. Struct. 152, 493–505 (2017). https://doi.org/10.1016/j.engstruct.2017.08.050

Challenging Glass 7
Conference on Architectural and Structural Applications of Glass
Belis, Bos & Louter (Eds.), Ghent University, September 2020.
ISBN 978-94-6366-296-3, www.challengingglass.com

PLATINUM SPONSORS

GOLD SPONSORS

SILVER SPONSORS

ORGANISING PARTNERS